Supplementary Information

Tracking Pyrolysis Process of a 3-MeOsalophen-ligand based Co_2 Complex for Oxygen Evolution Reaction

Bingxin Pan,[1] Xu Peng,*[1] Yifan Wang,[1] Qi An,[1] Xu Zhang,[1] Yuexing Zhang,[1] Thomas S. Teets[3] and Ming-Hua Zeng *[1,2]

1 Hubei Collaborative Innovation Center for Advanced Organic Chemical Materials, Ministry-of-Education Key Laboratory for the Synthesis and Application of Organic Functional Molecules & College of Chemistry & Chemical Engineering, Hubei University, Wuhan, 430062, P. R. China.

2 Department of Chemistry and Pharmaceutical Sciences, Guangxi Normal University, Key Laboratory for the Chemistry and Molecular Engineering of Medicinal Resources, Guilin, 541004, P. R. China.

3 Department of Chemistry, University of Houston, 3585 Cullen Boulevard, Room 112, Houston, Texas 77204-5003, United States.

E-mail: pengxu@hubu.edu.cn; zmh@mailbox.gxnu.edu.cn

Contents

Experimental Section

Characterization

Elemental analysis of C, H, and N microanalyses were carried out using an Elementar Vario-EL CHNS elemental analyzer. FT-IR spectra were recorded from KBr pellets containing 1 % of the compound in the range of 400-4000 cm^{-1} on a Bio-Rad FTS-7 spectrometer (**Figure S1**). The thermogravimetric analysis (TGA) were performed using a Pyris Diamond TG/DTA under a constant flow of dry nitrogen gas at a heating rate of 2 $°C·min^{-1}$. Powder X-ray diffraction (PXRD) spectra were recorded on either a D8 Advance (Bruker) or a Rigaku D/max-IIIA diffractometer (Cu Kα, λ = 1.54056 Å) at 293 K (**Figure S2)**. Transmission electron microscopy (TEM) and High-resolution TEM (HR-TEM) images of the samples were obtained using a FEI Talos F200X transmission electron microscope (200 kV). X-ray photoelectron spectroscopy (XPS) was conducted on VG Microtech ESCA 2000 using a monochromic Al X-ray source, and the binding energies (BE) were calibrated by setting the measured BE of C 1s to 284.8 eV. The N_2 adsorption-desorption isotherms were collected using a Quantachrome Instruments Autosorb-iQ2-MP at 77 K. Prior to the measurement, the samples were degassed at 200 ^{o}C. Raman spectra were collected by a Renishaw System 1000 micro-Raman spectroscope. Inductively coupled plasma optical emission spectroscopy was conducted on Agilent 720.

Synthesis of 3-MeOsalophen-ligand ligand

In a typical experiment, 1, 2-diaminobenzene (2.16 g, 20 mmol) and 3-methoxysalicylaldehyde (1.24 g, 10 mmol) was added to a round bottomed flask using ethanol as a solvent, and then stirred in a constant temperature oil bath at 80 °C for 3 h. After above reaction, the orange powder of 3-MeOsalophen ligand were washed with ethanol and collected by filtration, and finally dried in air.

Synthesis of Co_2 complex

$CoCl_2·6H_2O$ (0.5 mol, 0.118 g) was added to a solution of the 3-MeOsalophen ligand (0.5 mol, 0.188 g) in CH_3OH (10 mL). The mixture was stirred for 10 min before being added to a 25 mL Teflon-lined autoclave and then heated at 80 °C for 1 day. The autoclave was then cooled down to room temperature at a rate of 10 $°C·h^{-1}$, and brown crystals of **Co_2** complex were collected by filtration, washed with CH_3OH, and dried in air. Yield (based on Co): approx. 40 %. Anal. calcd. for $Co_2C_{25}H_{31}Cl_3N_2O_8$: C, 42.15; H, 4.35; N, 3.93 %. Found: C, 42.21; H, 4.32; N, 3.95 %. FT-IR (KBr, cm^{-1}): 3388 (m), 1614 (s), 1468(s), 1380 (s), 1320 (s), 1249 (s), 1200(s), 1108 (m), 981 (m), 736 (m), 535(w).

Synthesis of Co/CoO_x@NCs from Co_2 complex with different pyrolysis condition

The aforementioned of **Co_2** complex was transferred into a quartz boat in the center of a tube furnace and annealed at under an Ar flow. The measurements were conducted from room temperature to target temperature with 5 $K·min^{-1}$ gradient. The samples were cooled down to room temperature for other tests.

Synthesis of Co/CoO_x@NCs from Co_2 complex with different pyrolysis condition

The aforementioned of **Co_2** complex was transferred into a quartz boat in the center of a tube furnace and annealed at under an Ar flow. The measurements were conducted from room temperature to target temperature with 5 K·min^{-1} gradient. The samples finally cooled down to room temperature for other tests.

X-ray Crystallography

Single crystals of compound were collected on a XtaLAB Synergy with graphite monochromated Mo-Kα radiation (λ = 0.71073 Å) at 100(2) K. The intensity data were corrected for Lorentz and polarization effects (SAINT), and empirical absorption corrections based on equivalent reflections were applied (SADABS). The structures were solved by direct method and refined on F^2 by full-matrix least-squares method with SHELXTL program package. All non-hydrogen atoms were refined with anisotropic thermal parameters, and the hydrogen atoms of organic cations were generated theoretically onto the specific carbon atoms and refined isotropically with fixed thermal factors. The crystallographic details are provided in **Table S1**, and selected bond lengths and angles are given in **Table S2**. CCDC reference numbers 1882936.

Thermogravimetric Analysis Combined with Mass Spectrometry (TG-MS)

The thermogravimetric analysis was performed on a Rigaku Thermo Mass Photo (TG-MS) with a Skimmer type mass spectrometer (MS/EI). The measurements were conducted from 20-800 ^{o}C with 5 K·min^{-1} gradient, after which the samples were cooled down to room temperature. The weight of initial samples was about 3.0 mg, and the pyrolysis process was conducted under a helium gas flow of 300 mL·min^{-1}.

Electrochemical tests

The electrochemical and electrocatalytic properties of the materials toward OER were comprehensively evaluated with a traditional three-electrode configuration using an electrochemical station (CHI 760E) in 1 M KOH solutions at room temperature. In our case, carbon paper uniformly coated with the electrocatalysts was used as the working electrode, an Hg|Hg_2Cl_2 (saturated KCl solution) electrode was used as reference electrode, while the counter electrode was a graphite rod electrode. The geometric area of the carbon paper was used to normalize the current density. The working electrode was prepared using the following procedure. Typically, 3.0 mg as-obtained Co@CoO_x-NCs material was first dispersed in 300 μL of 2-propanol and 200 μL CH_3OH mixture under sonication for 30 minutes to form a homogeneous suspension or ink. Then, 70 μL of the resulting dispersion was pipetted using a micropipette and drop-casted onto the surface of a carbon paper with the area of 0.25 cm^2, leading a catalyst loading of 1.68 mg·cm^{-2}. After letting the catalyst-coated electrode surface dry under atmospheric conditions, 2 μL of Nafion (5 % in 2-propanol) solution was drop-casted on the top of the electrode to protect the catalyst. The electrode was then allowed to completely dry under ambient conditions. The working electrodes underwent 20 cycles of cycle voltammetry until stabilization of current before data collection. Electrochemical

impedance spectroscopy (EIS) measurements of the catalysts were conducted at a potential of 1.6 V ***vs*** RHE in a frequency range from 10 kHz to 100 mHz by using an AC voltage with 5 mV amplitude. Double layer capacitance (C_{dl}) of all the as-obtained samples was measured in 1 M KOH solution. Then, five CVs with different scan rates (2, 4, 6, 8, 10 and 12 $mV \cdot s^{-1}$) were obtained in a potential window of 0.1 to 0.2 V, in which no Faradaic process occurs and the current emerges mainly from the double layer capacitance.

Table S1. Crystallographic data for compound **Co_2**.

Compounds	**Co_2**
Formula	C_{23} H_{23} Cl_3 Co_2 N_2 O_6
Formula weight	647.63
T (K)	293
Crystal system	monoclinic
Space group	$P2_1/c$.
a (Å)	14.9719(4)
b (Å)	7.6746(3)
c (Å)	24.3948(6)
α (°)	90
β (°)	91.371(3)
γ (°)	90
V (Å^3)	2802.24(15)
Z	4
D_c.(g cm^{-3})	1.530
μ (mm^{-1})	12.243
Reflns coll.	15871
Unique reflns	6093
R_{int}	0.0483
$R_1{}^a$[I ≥ 2σ(I)]	0.0854
$wR_2{}^b$ (all data)	0.2561
GOF	1.041

$^aR_1 = \sum||F_o| - |F_c||/\sum|F_o|$. $^bwR_2 = [\sum w(F_o^2 - F_c^2)^2/\sum w(F_o^2)^2]^{1/2}$.

Table S2. Selected Bond lengths (Å) and angles (°) for compound **Co_2**.

Co1-Cl1	2.271(17)	Co1-Cl2	2.274(17)	Co1-O1	1.900(4)	Co1-O2	1.889(4)
Co1-N1	1.878(4)	Co1-N2	1.882(4)	Co2-O1	2.235(4)	Co2-O2	2.122(4)
Co2-O5	2.089(5)	Co2-O6	2.058(5)	Co2-Cl3	2.326(19)	Cl1-Co1-Cl2	178.590(6)
O1-Co1-Cl1	90.680(13)	O1-Co1-Cl2	90.590(13)	N1-Co1-Cl1	89.960(15)	N1-Co1-O1	96.830(19)
N1-Co1-Cl2	89.270(15)	N1-Co1-O2	177.860(18)	N1-Co1-N2	85.860(19)	O2-Co1-Cl1	90.410(13)
O2-Co1-Cl1	81.060(16)	O2-Co1-Cl2	90.410(13)	N2-Co1-Cl1	89.040(14)	N2-Co1-O1	177.300(18)
N2-Co1-Cl2	89.730(14)	N2-Co1-O2	96.260(17)	O1-Co2-Cl3	140.350(12)	O2-Co2-O1	68.780(14)
O2-Co2-Cl3	150.870(12)	O5-Co2-O1	85.740(19)	O5-Co2-O2	87.230(18)	O5-Co2-Cl3	93.930(15)
O6-Co2-O1	87.200(2)	O6-Co2-O2	85.880(18)	O6-Co2-Cl3	94.460(16)	O6-Co2-O5	171.600(2)

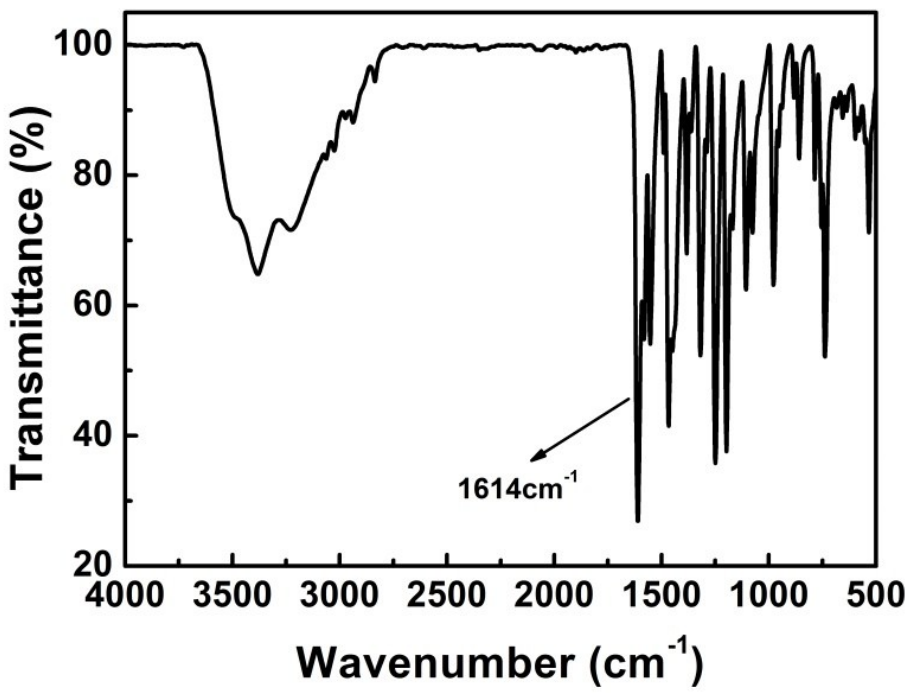

Figure S1. The IR spectrum for compound for **Co_2**.

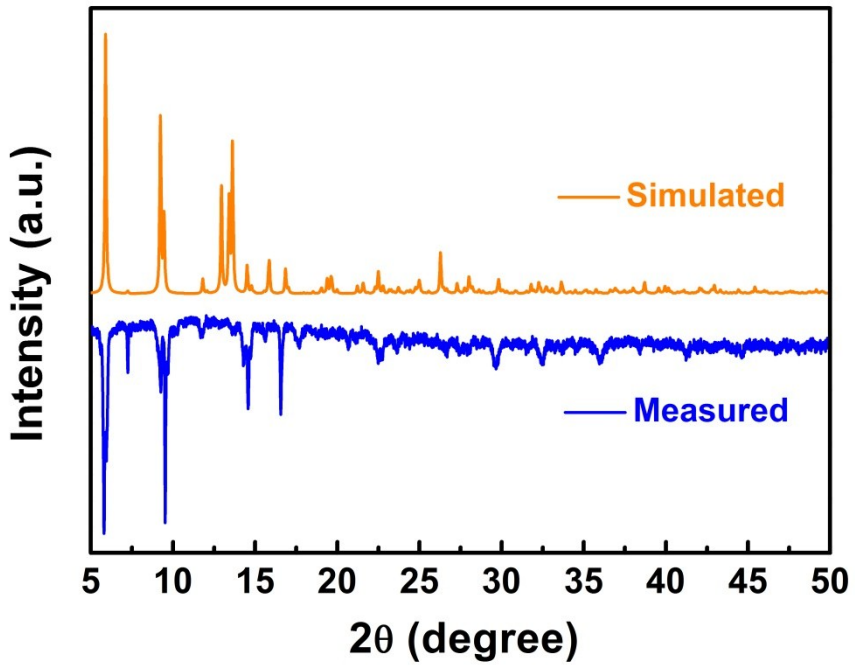

Figure S2. Experimental and simulated PXRD patterns for **Co_2.**

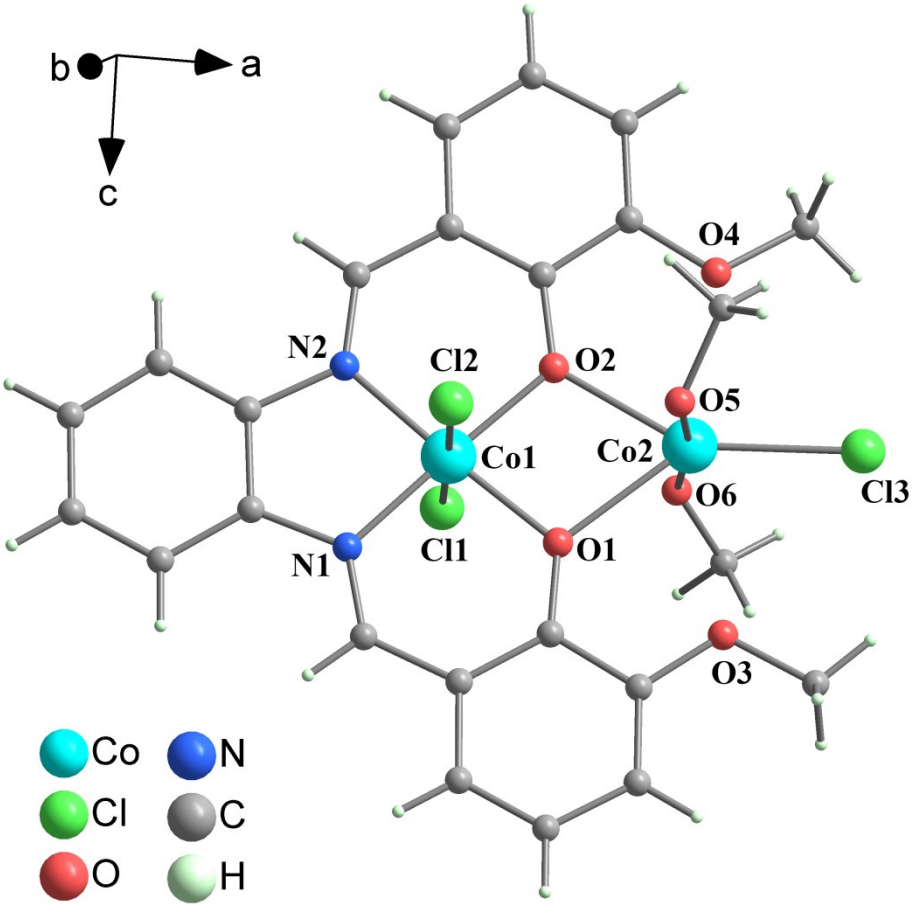

Figure S3. View of the **Co_2** Complex showing the intramolecular.

Table S3. The specific phase changes and facets information for Co/CoO_x@NCs.

Phases / Samples	**Cubic Co** JCPDS 15-0806	**Hexagonal Co** JCPDS 05-0727	**CoO** JCPDS 43-1004	**Co_3O_4** JCPDS 43-1003
Co/CoO_x@NC-500	(111) (200) (220)	(100) (002)	/	/
Co/CoO_x@NC-600	(111) (200) (220)	/	(111) (200) (220)	/
Co/CoO_x@NC-700	(111) (200) (220)	/	(111) (200) (220) (311) (222)	(220) (311) (511) (440)
Co/CoO_x@NC-800	(111) (200) (220)	/	(111) (200) (220) (311) (222)	/
Co/CoO_x@NC-900	(111) (200) (220)	/	(111) (200) (220) (311) (222)	(111)(220)(311)(222)(400) (422)(511)(440)

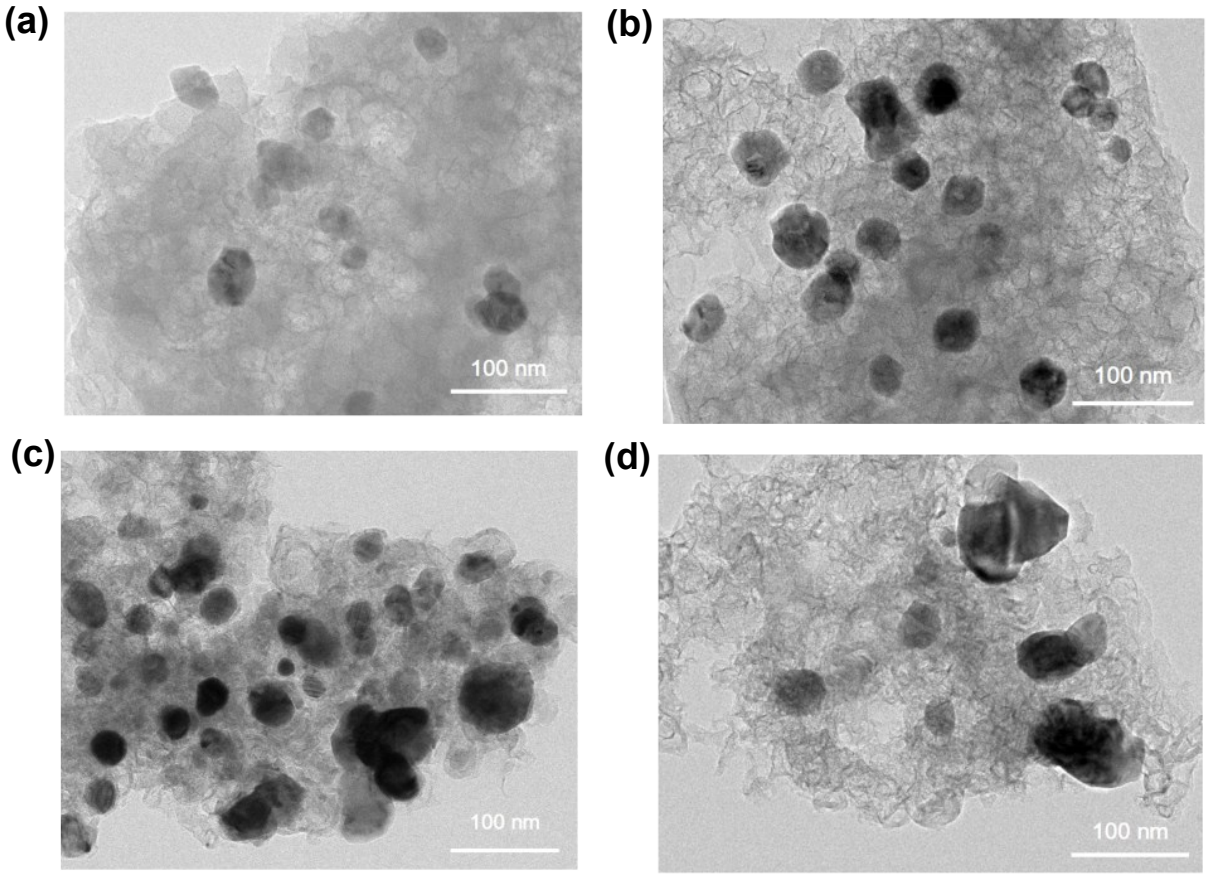

Figure S4. TEM images of the Co/CoO_x@NCs at different pyrolysis temperatures: (a) Co/CoO_x@NC-600, (b) Co/CoO_x@NC-700, (c) Co/CoO_x@NC-800, (d) Co/CoO_x@NC-900.

In this manuscript, pyrolysis temperature indeed plays a key role on the final catalytic performance. In order to further make clearer our results, we have made systematically explanations as below.

1. TG-MS along with TEM confirms the study range of pyrolysis temperature is 600-900 ^{o}C

According to the TG-MS analysis (Figure 3b), when the temperature rises to a temperature of about 600 ^{o}C, no new fragments are detected, thus the violent decomposition and recombination process has basically stopped. Meanwhile, it can be seen from the TEM (Figure S4) images that the core-shell structure which is favorable for electrocatalysis has been formed. Therefore, we further systematically study the pyrolysis temperature range from 600-900 ^{o}C to explore the best pyrolysis temperature for superior catalytic performance.

2. Further characterization confirms the differences of nanostructures among 600-900 ^{o}C on catalytic performance

We conducted XPS (Figure 2a-d), Raman spectroscopy (Figure 2e) and BET surface area (Figure 2f), showing

that pyrolysis temperature could influence the ratio of Co^{2+}/Co^{3+}, ratio of I_D/I_G and BET surface areas in different Co/CoO_x@NC samples, leading to effect on catalytic performance. In our case, Co/CoO_x@NC-800 sample has higher Co^{2+}/Co^{3+} and reasonable I_D/I_G ratios as well as relatively higher BET surface areas compared with other Co/CoO_x@NCs. And above merits are all beneficial for realizing superior catalytic performance. Interestingly, we combined the results of TG-MS and found that a reductive atmosphere was detected when pyrolysis temperature between 520-700 ^{o}C, further answering for the higher Co^{2+}/Co^{3+} ratios and relatively higher BET surface areas.

Table S4. Elemental quantification determined by XPS for Co/CoO_x@NCs.

Elements / Samples	C (at %)	N (at %)	O (at %)	Co (at %)
Co/CoO_x@NC-600	79.49	6.54	10.77	3.2
Co/CoO_x@NC-700	89.61	3.39	5.63	1.37
Co/CoO_x@NC-800	91.08	2.2	5.29	1.42
Co/CoO_x@NC-900	83.32	3.35	11.47	1.87

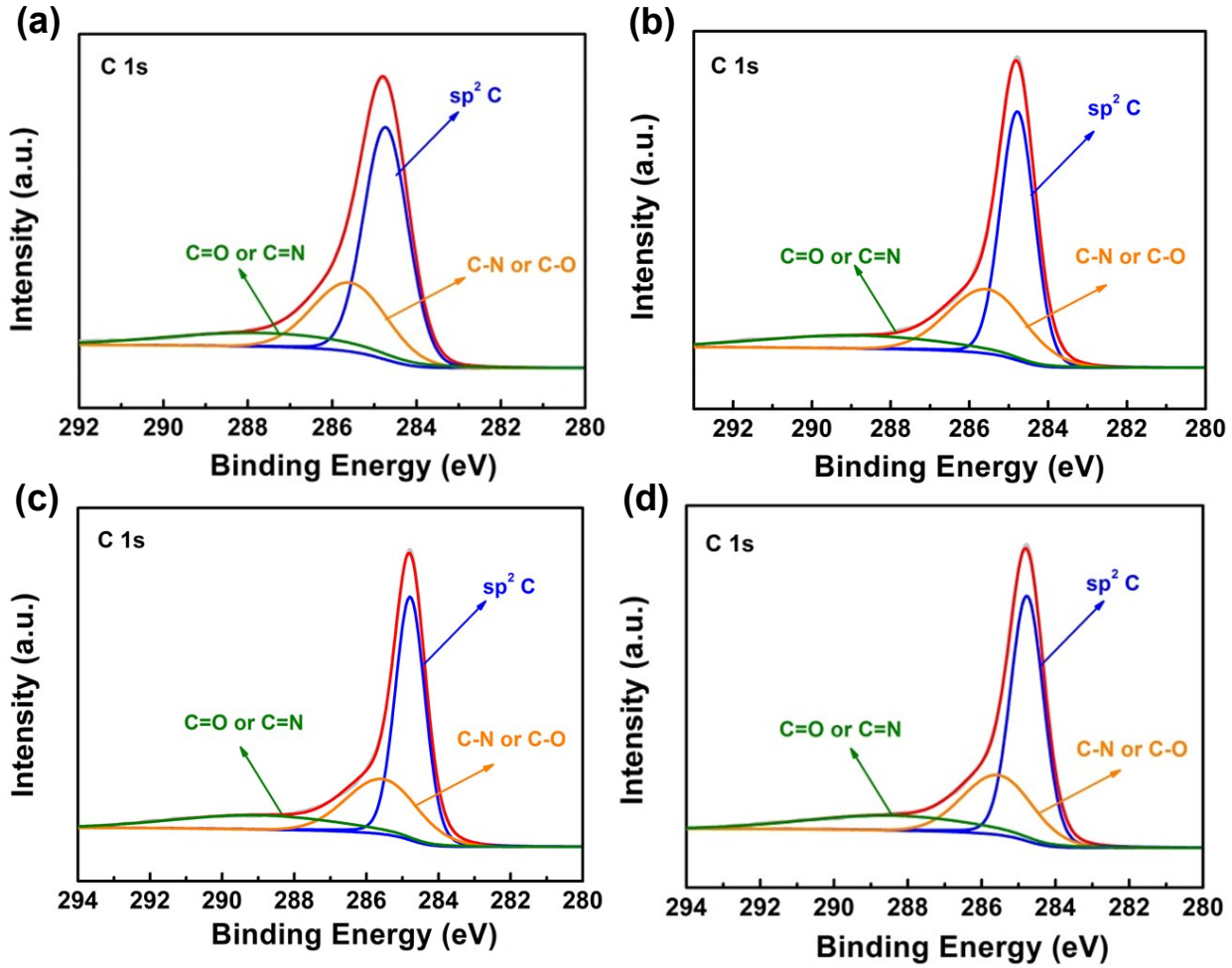

Figure S5. High resolution XPS spectra of C 1s peak of Co/CoO_x@NCs at different pyrolysis temperatures: (a) Co/CoO_x@NC-600, (b) Co/CoO_x@NC-700, (c) Co/CoO_x@NC-800, (d) Co/CoO_x@NC-900.

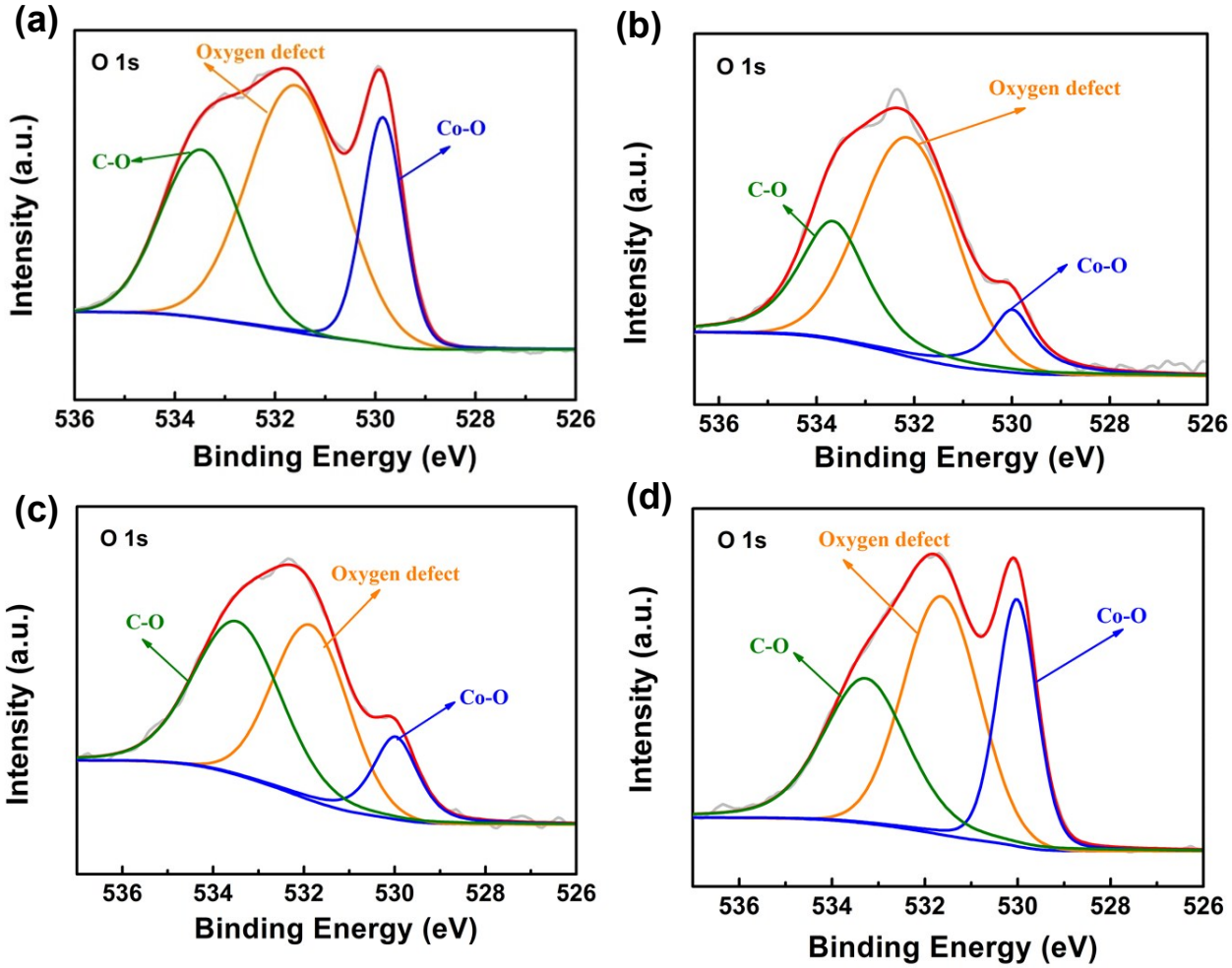

Figure S6. High resolution XPS spectra of O 1s peak of Co/CoO_x@NCs at different pyrolysis temperatures: (a) Co/CoO_x@NC-600, (b) Co/CoO_x@NC-700, (c) Co/CoO_x@NC-800, (d) Co/CoO_x@NC-900.

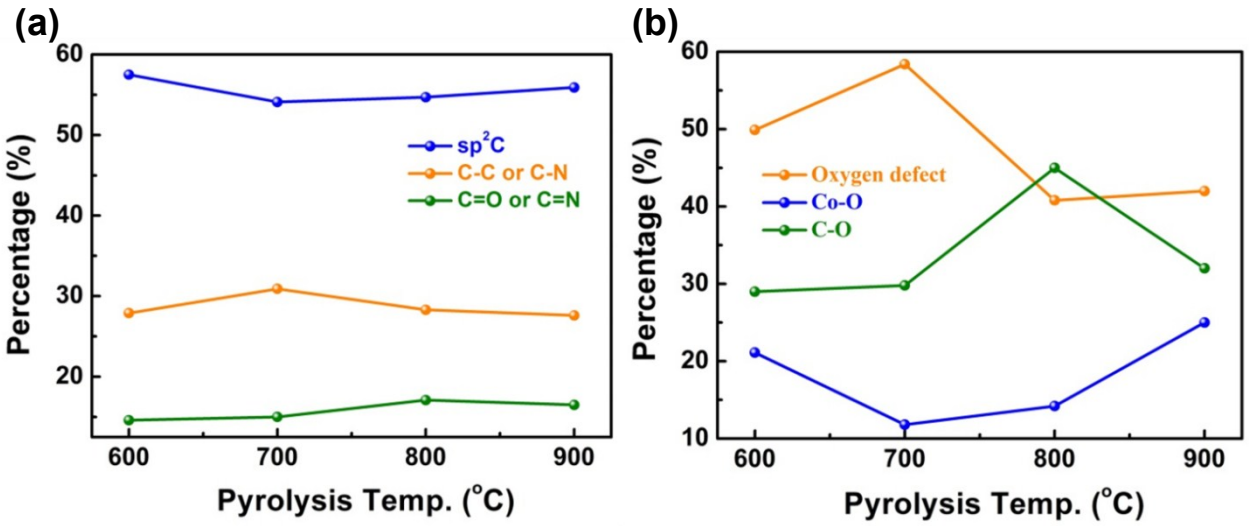

Figure S7. Composition of Co/CoO_x@NCs as a function of their pyrolysis temperatures: percentages of the different: (a) C and (b) O species present in Co/CoO_x@NCs.

Table S5. Fitting results for C 1s spectra of various catalysts with different pyrolysis temperatures.

Species / Samples	**sp^2C (%)**	**C-N or C-O (%)**	**C=N or C=O (%)**
	284.6 eV	**285.6 eV**	**287.5 eV**
Co/CoO_x@NC-600	57.5	27.9	14.6
Co/CoO_x@NC-700	54.1	30.9	15.0
Co/CoO_x@NC-800	54.7	28.3	17.1
Co/CoO_x@NC-900	55.9	27.6	16.5

Table S6. Fitting results for O 1s spectra of various catalysts with different pyrolysis temperatures.

Species / Samples	Oxygen defect (%)	Co-O (%)	C-O (%)
	531.6 eV	**529.8 eV**	**533.5 eV**
Co/CoO_x@NC-600	49.9	21.1	29.0
Co/CoO_x@NC-700	58.4	11.8	29.8
Co/CoO_x@NC-800	40.8	14.2	45.0
Co/CoO_x@NC-900	42.0	25.0	32.0

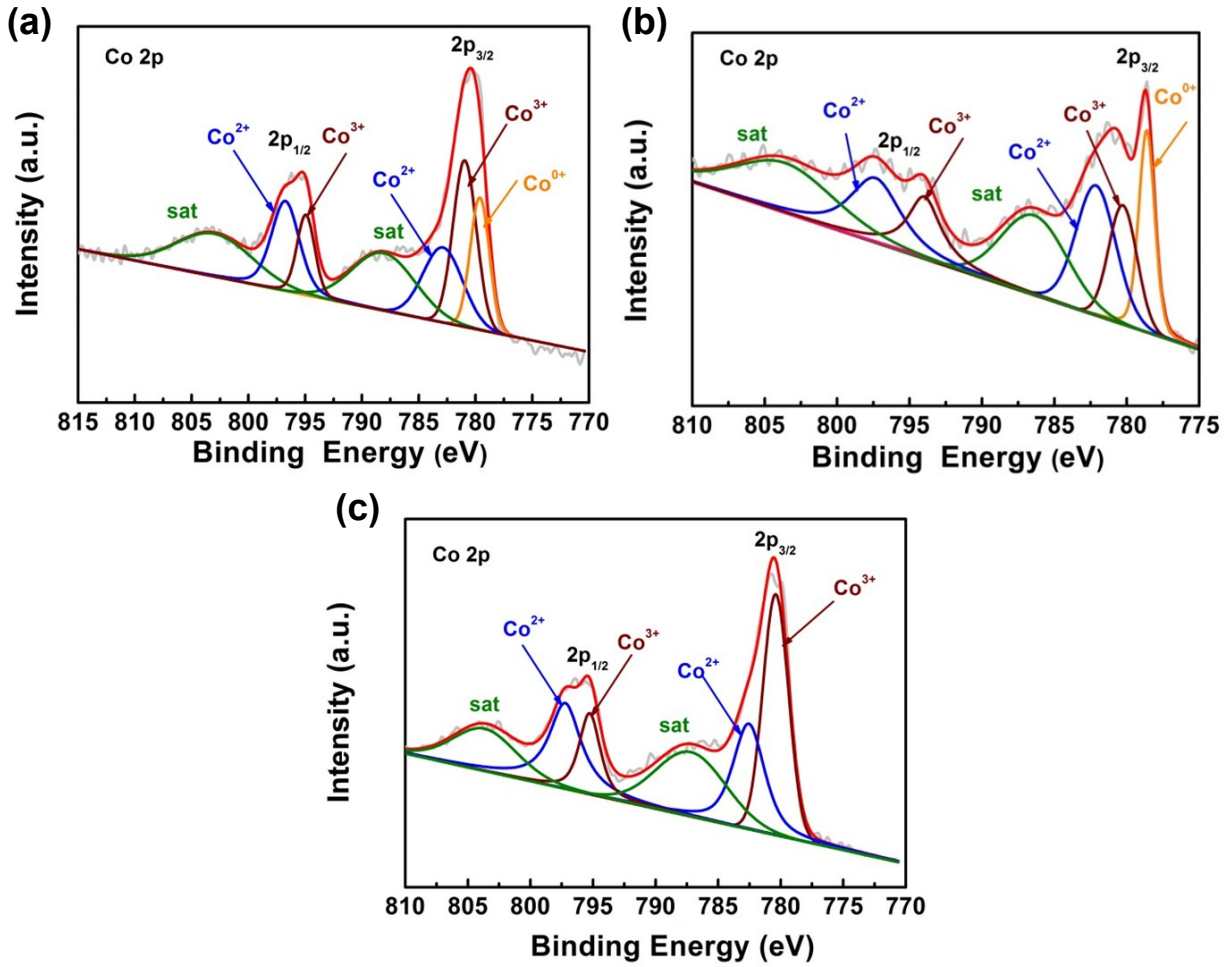

Figure S8. High resolution XPS spectra of Co 2p peak of Co/CoO_x@NCs at different pyrolysis temperatures: (a) Co/CoO_x@NC-600, (b) Co/CoO_x@NC-700, (c) Co/CoO_x@NC-900.

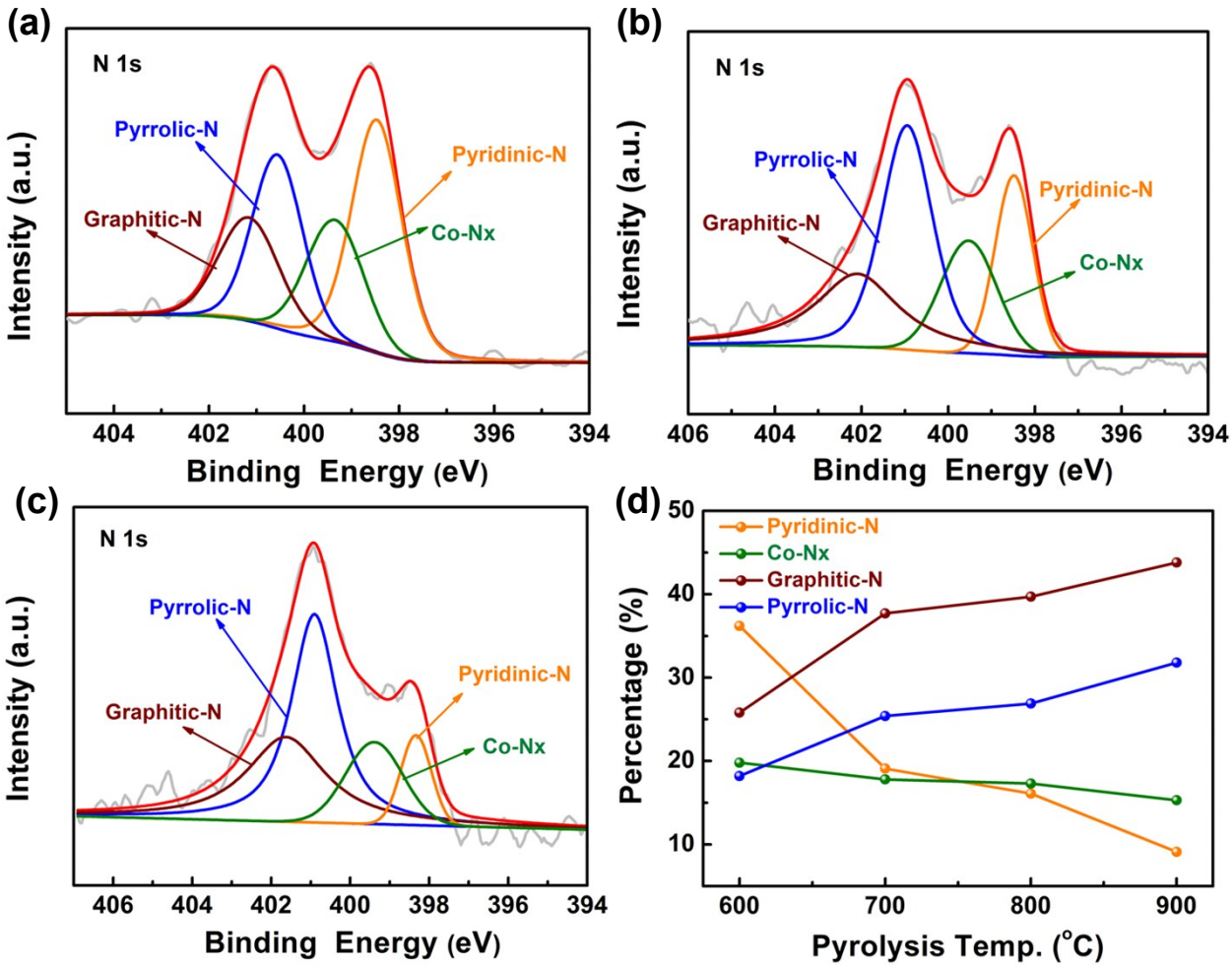

Figure S9. High resolution XPS spectra of N 1s peak of Co/CoO_x@NCs at different pyrolysis temperatures: (a) Co/CoO_x@NC-600, (b) Co/CoO_x@NC-700, (c) Co/CoO_x@NC-900 and (d) N species present in Co/CoO_x@NCs.

Table S7. Fitting results for N 1s spectra of various catalysts with different pyrolysis temperatures.

Species / Samples	**Graphitic-N (%)**	**Co-N_x (%)**	**Pyridine-N (%)**	**Pyrrolic-N (%)**
	401.2 eV	398.5 eV	399.4 eV	400.6 eV
Co@CoO_x/NC-600	18.2	19.8	36.2	25.8
Co@CoO_x/NC-700	25.4	17.8	19.1	37.7
Co@CoO_x/NC-800	26.9	17.3	16.1	39.7
Co@CoO_x/NC-900	31.8	15.3	9.1	43.8

Table S8. The Co content in Co/CoO_x@NCs was determined by inductively coupled plasma optical emission spectroscopy.

Samples / **Elements**	Co (wt%)
Co/CoO_x@NC-600	35.75
Co/CoO_x@NC-700	50.42
Co/CoO_x@NC-800	40.49
Co/CoO_x@NC-900	68.42

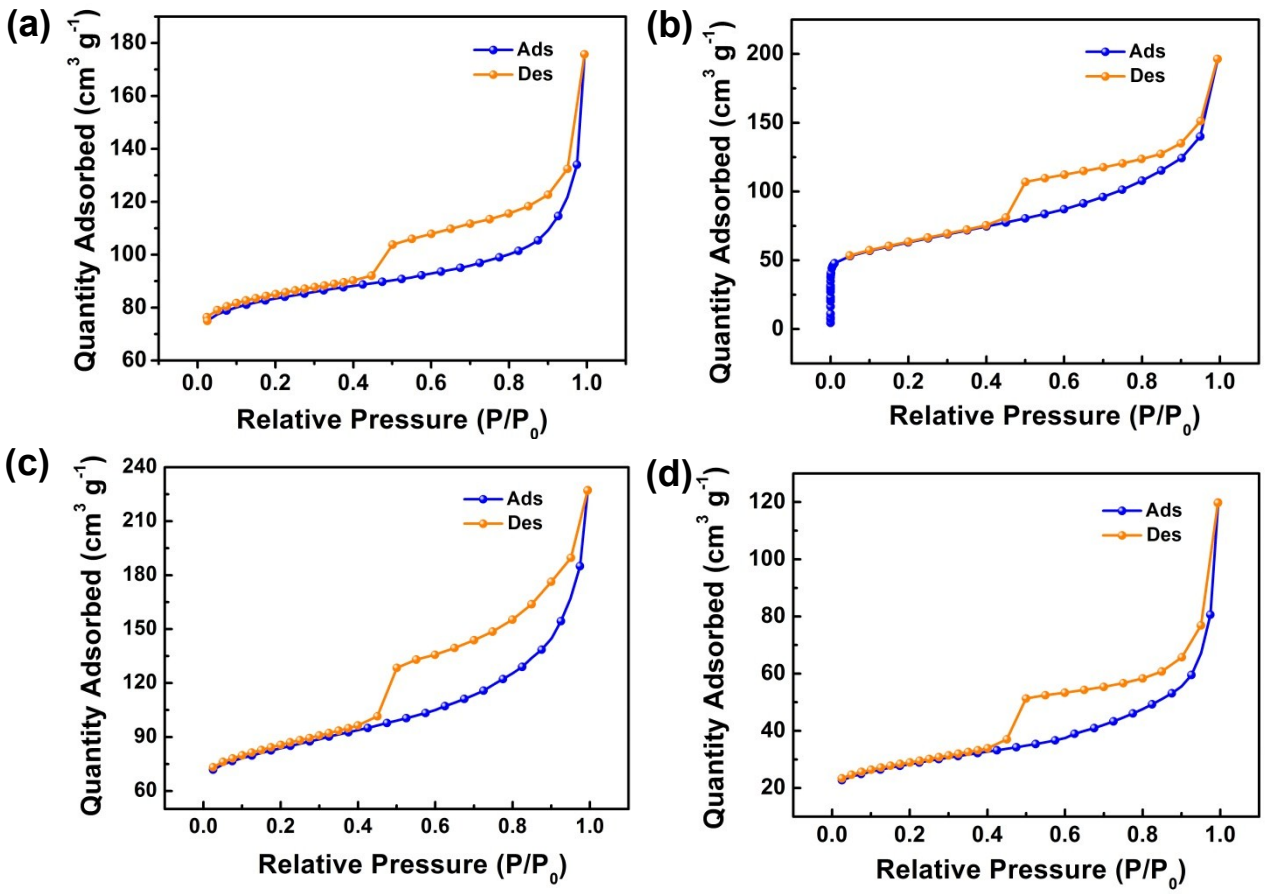

Figure S10. N_2 sorption isotherms of the Co/CoO_x@NCs at 77 K: (a) Co/CoO_x@NC-600, (b) Co/CoO_x@NC-700, (c) Co/CoO_x@NC-800, (d) Co/CoO_x@NC-900.

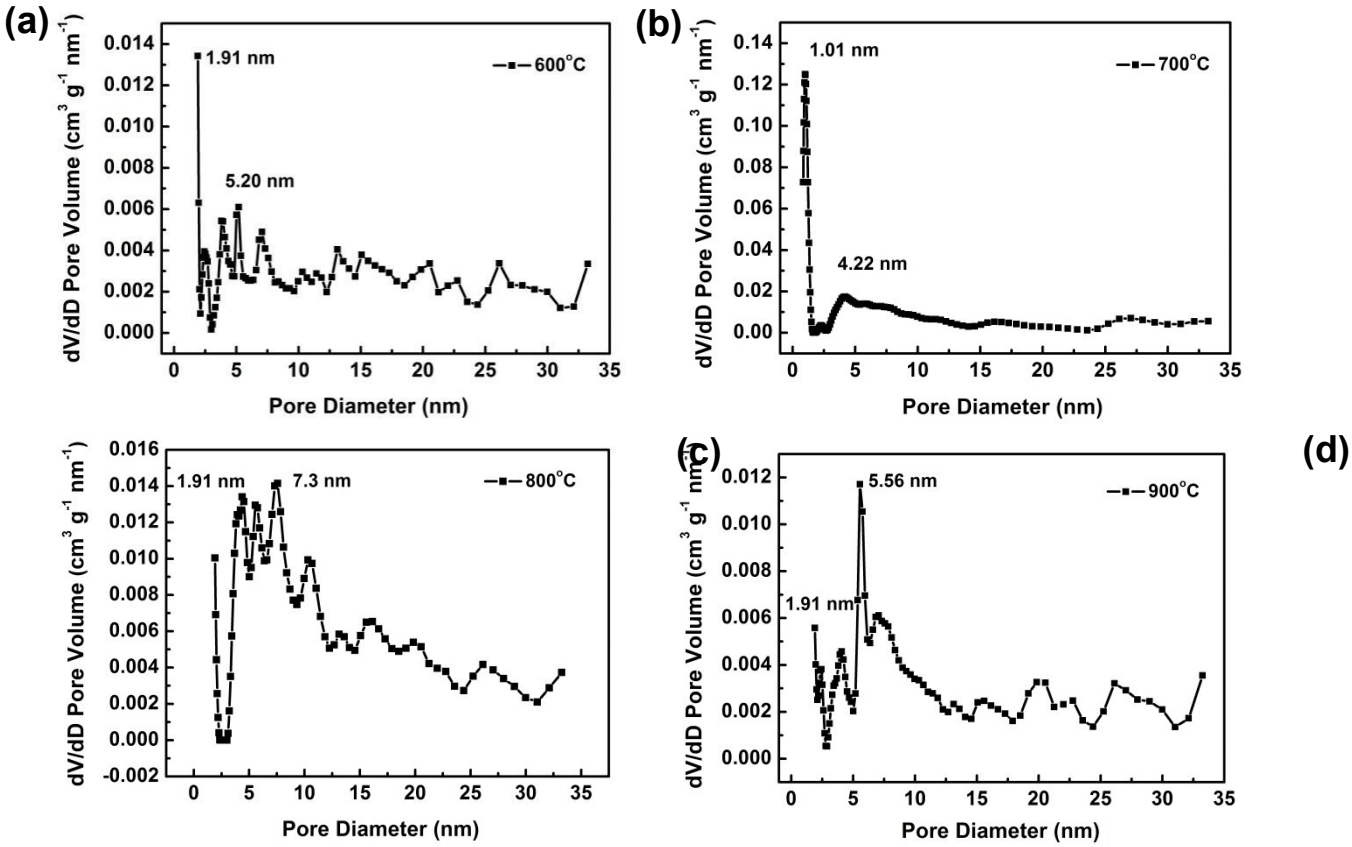

Figure S11. Related pore size distribution of the Co/CoO_x@NCs by the QSDFT method: (a) Co/CoO_x@NC-600, (b) Co/CoO_x@NC-700, (c) Co/CoO_x@NC-800, (d) Co/CoO_x@NC-900.

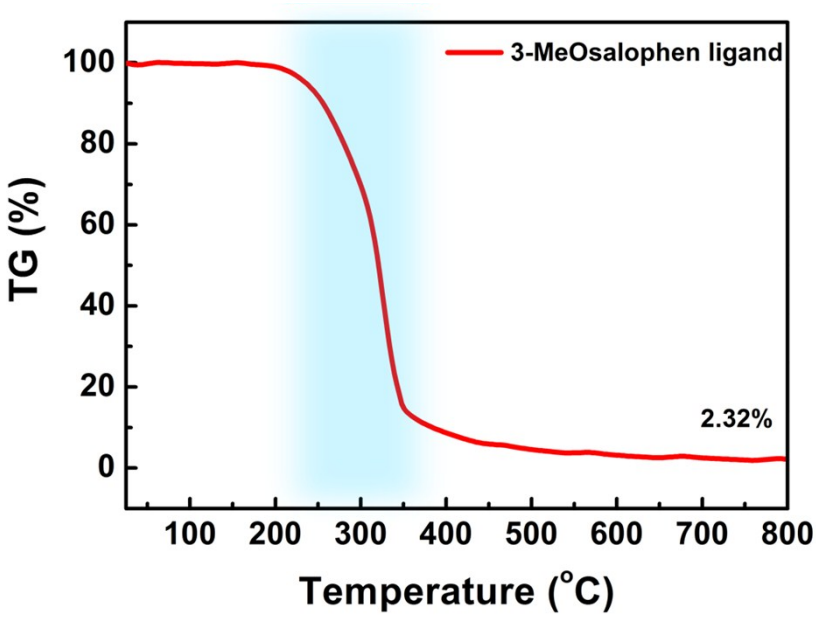

Figure S12. TG profile of 3-MeOsalophen-ligand (Bis[3-Methoxysalicylydene]-1,2 Iminophenylenediamine).

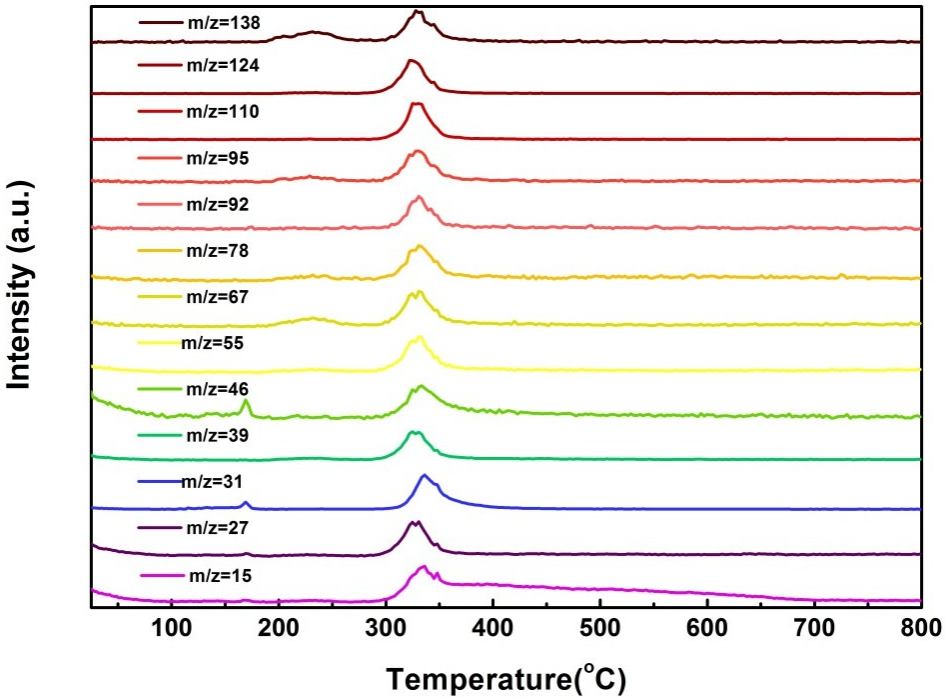

Figure S13. TG-MS curves of corresponding 3-MeOsalophen-ligand pyrolysis tracking process. The fragments m/z = 15 (CH_3), m/z = 31 (CH_3O), m/z=78 (C_6H_6) and m/z=39, 46, 55, 67, 92, 95, 110, 124, 138 (Fragments produced by the decomposition of 3-MeOsalophen-ligand frameworks).

Table S9. Representative Co-based OER electrocatalyst using pyrolysis treatment forming Co/CoO_x@NC nanostructures from different kinds of Co precursors.

Materials	**Precursors**	**Methods**	**$\eta_{10\ mA\cdot cm^{-2}}$ (mV)**	**Tafel slope (mV decade^{-1})**	**References**
Co_9S_8@NOSC	**$(NH_4)_2S_2O_8$, S-PPY, HCl**	Pyrolysis	340	68	*Adv. Funct. Mater.* **2017**, *27*, 1606585.
Core–shell Co@NC	**$Co_3[Co(CN)_6]_2\cdot nH_2O$-PB**	Pyrolysis	280	62.5	*Adv. Energy Mater.* **2018**, 1702838.
Core–shell Co@Co_3O_4 nanoparticles	**ZIF 67**	Pyrolysis	1.64 V (RHE) 0.1 M KOH	54.3	*Angew. Chem. Int. Ed.* **2016**, *55*, 4087.
Co@CoO_x nanoparticles	**$Co(OAc)_2\cdot 4H_2O$, diethyl oxalate ethanol**	Heat treatment	289	68.9	*Chem. Commun.* **2017**, *53*, 9277.
MOF-Derived Co@N-C	**Co-based MOF**	Pyrolysis	350	79	*Adv. Mater.* **2018**, *30*, 1705431.
Mononuclear CoII Coordination Complex	**Co-based MOF**	/	390 mV at 1 mA·cm^{-2} (vs. NHE) 0.1M KOH	128	*Angew. Chem. Int. Ed.* **2016**, *55*, 2425.
Co/CoO@Co–N-C	**shrimp-shell, Co salt**	Pyrolysis	0.63 V (vs. Ag/AgCl) 0.1M KOH	/	*Chem. Commun.* **2016**, *52*, 5946.
Complex derived Co/CoO_x@NC	**3-MeOsalophen-ligand-ligand based Co_2**	**TG-MS Pyrolysis**	**288**	**98**	**Our work**

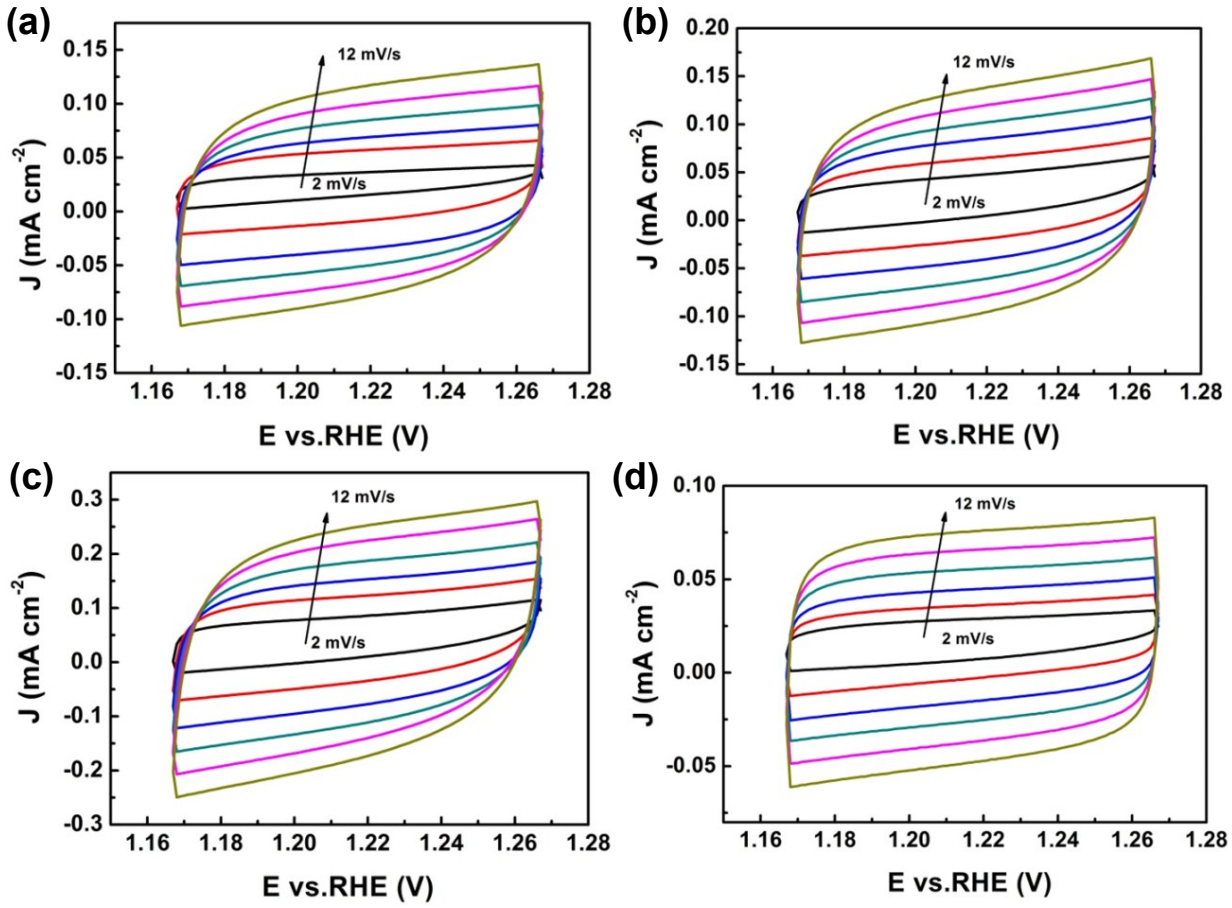

Figure S14. Cyclic voltammograms (CVs) measured over Co/CoO_x@NCs modified electrodes in the double layer capacitance charging region at scan rates of 2, 4, 6, 8, 10 and 12 mV·s^{-1} in 1.0 M aqueous KOH electrolyte. The materials include: (a) Co/CoO_x@NC-600, (b) Co/CoO_x@NC-700, (c) Co/CoO_x@NC-800, (d) Co/CoO_x@NC-900.

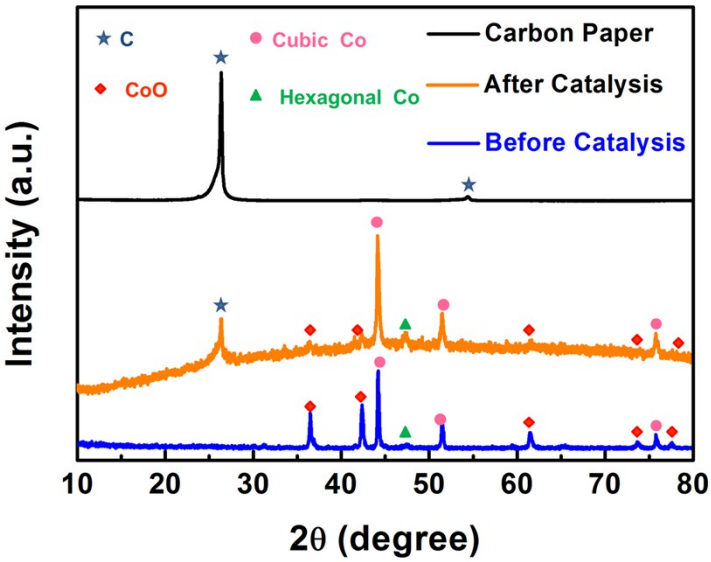

Figure S15. Powder XRD patterns of Co/CoO_x@NC-800 before and after the catalysis, as well as the carbon paper.